Characterization of a hybrid Al2O3–aluminum matrix composite manufactured via composite extrusion

A. Reeb, V. Walter, V. Schulze, Kay A. Weidenmann

Angaben zur Veröffentlichung / Publication details:

Reeb, A., V. Walter, V. Schulze, and Kay A. Weidenmann. 2016. "Characterization of a hybrid Al2O3–aluminum matrix composite manufactured via composite extrusion." *Journal of Composite Materials* 50 (8): 1099–1108. https://doi.org/10.1177/0021998315587317.

Characterization of a hybrid Al_2O_3–aluminum matrix composite manufactured via composite extrusion

A Reeb, V Walter, V Schulze and KA Weidenmann

Abstract

The development of new metal matrix composites for lightweight applications is aiming for an increase in specific strength and stiffness compared to conventional light metal alloys. The composite extrusion process is a promising manufacturing method for continuously reinforced light metal profiles. Especially the reinforcement with ceramic fibers leads to an increase in the specific strength and stiffness. For these investigations a hybrid composite is produced by using an Al_2O_3-fiber/AlMg0.6 composite wire which is embedded in an EN AW-6082 aluminum matrix. It is shown that the mechanical properties of the composite exceed those of the unreinforced matrix material. An explicit investigation of the deformation and damage behavior of this composite is given by optical strain analysis and in situ tensile tests in an X-ray micro computed tomograph (μ-CT). It was observed that during tensile loading multiple fracture of the composite wire occurs while exceeding the strain limit of the non-embedded composite wire. It could be shown that fracture of the composite wire is accompanied by strain localization and therefore strain hardening occurs in vicinity of the internal fracture, which leads to multiple necking of the specimen. The μ-CT analysis reveals the intrinsic damage mechanisms and shows the beginning of ceramic fiber fracture which showed evidence for a local load distribution between the fibers resulting in a planar fracture of the composite wire. The multiple fracture of the wire allows for an interface shear strength analysis and indicates a good bonding of the composite wire.

Keywords

Metal matrix composite wires, composite extrusion, Altex fibers, lightweight structures, damage analysis, interface characterization

Introduction

Motivation

As a consequence of limited energy resources and fossil fuels, development of new lightweight materials for automotive and aviation applications becomes indispensable for slowing down the global fuel consumption. For improving materials for lightweight applications one aim is to increase specific mechanical properties like specific stiffness or specific strength. Metal matrix composites with light metal matrices therefore play an important role. One strategy for producing unidirectional reinforced light metal matrix composites is the composite extrusion process.[1,2] This process allows a rapid and flexible production of aluminum profiles with improved mechanical and functional properties.

The composite extrusion process is illustrated in Figure 1. During the process, reinforcement elements, like steel wires, ropes or flat ribbons, are fed into the material flow by using modified porthole dies. First the conventional billet is split in front of the sealing plate into multiple strands which join again in the welding chamber. In between the reinforcing elements are fed from outside (with a deflection angle of 90°). The bonding between the billet material and the reinforcing element occurs under high temperature (400–500°C) and pressure (50–100 MPa) in the welding chamber.

Institute of Applied Materials (IAM-WK), Karlsruhe Institute of Technology, Karlsruhe, Germany

Corresponding author:
A Reeb, Institute of Applied Materials (IAM-WK), Karlsruhe Institute of Technology, Karlsruhe 76131, Germany.
Email: andreas.reeb@kit.edu

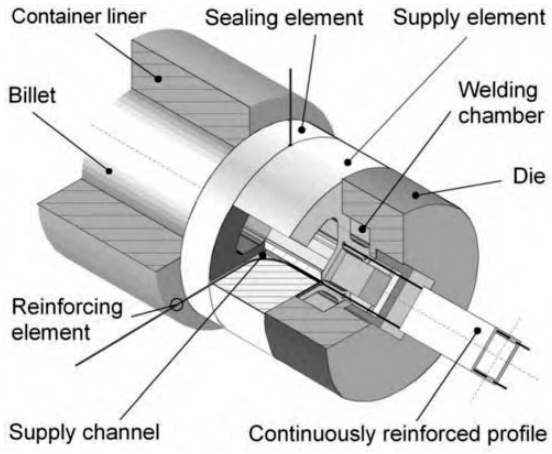

Figure 1. Principle of composite extrusion process.

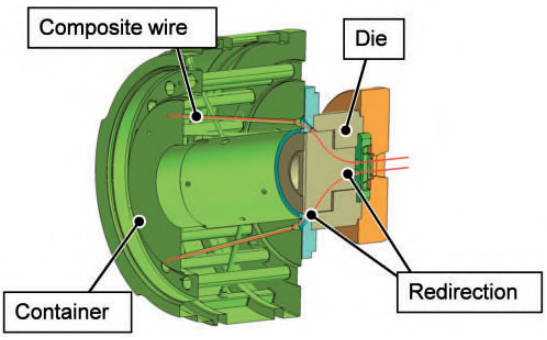

Figure 2. Feeding design for processing of composite wires according to Dahnke et al.[16]

Characterization of composite extruded profiles

Reinforcing aluminum and magnesium alloys with high strength steel wires by composite extrusion and the effect of reinforcement on the mechanical properties is well investigated in the collaborative research center SFB/Transregio 10 for the past 12 years. The project covered issues of material selection and processing for composite extrusion and the characterization, as well as the simulation of the resulting mechanical properties.[3–9] The main aim was therefore to improve the lightweight potential of extruded profiles. Essential work for material selection and characterization was done by Weidenmann with focus on steel wire reinforced EN AW-6060.[3,4] Using steel wire as reinforcing material allows for simple processing and leads to a significant increase in absolute stiffness and strength, and additionally to an increased fatigue endurance.[5–9] The disadvantage of steel wire as reinforcing element is its high density resulting in a reduced effectiveness regarding the specific properties and the lightweight potential. Especially the specific stiffness of composite extruded aluminum profiles cannot be increased by using steel wire.

Therefore high strength and stiff reinforcing materials with a low density are needed. For this purpose inorganic reinforcing elements such as ceramic and carbon fibers can meet these requirements.[10] The risk of interfacial corrosion is high when using carbon fibers in an aluminum matrix. Therefore ceramic alumina (Al_2O_3)-fibers were used within this investigation. In general, ceramic fibers cannot withstand shear or tensile stresses occurring during composite extrusion due to the lack of internal load transfer within the fiber bundle or yarn. In order to process these fibers the fiber-bundles have to be pre-infiltrated with an aluminum matrix, resulting in a composite wire which can then be processed by composite extrusion.[11,12] Such composite wire can then serve as an appropriate reinforcement for the composite extrusion process providing a good internal load transfer and avoid interfacial problems when using the same matrix material as for the composite extrusion profile. Previous investigations not only showed promising results in mechanical properties but also revealed difficulties in embedding of composite wires by the composite extrusion process[13–16] due to the high stiffness and brittle behavior. In this investigation a new tool design is used for embedding composite wires in a reliable manner which is further described in ''Composite extrusion with composite wires'' section.

Composite extrusion with composite wires

Due to the low ductility and high stiffness of these composite wires the feeding from outside with a deflection of 90° is challenging and can lead to fracture of the elements if bending radii are too small. Additionally the friction conditions inside the supply element have to be taken into account as the high temperatures causing high friction between the aluminum matrix of the wire and the die material (steel).[15,16] To reduce bending stresses and friction during feeding of the elements a new feed concept was developed by Dahnke et al.[16] (Figure 2).

In this concept the composite wires are fed through boreholes in the container of the extrusion press which reduces the bending radius of the composite wires significantly. In addition, for an improvement of the friction conditions and reducing the angle for redirecting the wires in the die a new feeder is used which contains additional silicon carbide bearings which redirect the wire through the die.[16] With these modifications of the composite extrusion process a continuous production of composite wire reinforced aluminum profiles is possible and a sufficient sample size for characterization could be produced.

As the resulting structure of such a hybrid composite is relatively complex, with various internal interfaces a

Table 1. Chemical analysis of the used EN AW-6082 alloy (AlMgSi1).

	Si	Fe	Cu	Mn	Mg	Cr	Ni	Zn	Ti	Other	Al
EN AW-6082 matrix	0.895	0.209	0.01	0.464	0.691	0.006	0.005	0.004	0.011	<0.15	Rest

focus of this work is the investigation and documentation of the damage mechanisms alongside the determination of mechanical properties. For this purpose the produced hybrid composite is characterized by metallographic investigations and tensile tests accompanied by optical strain analysis and by in situ computed tomograph (CT) analysis using a specially designed testing setup.

Materials and experimental setup

Materials

Within the current investigations, profiles with a cross-section of $40 \times 12\,mm^2$ were reinforced with one composite wire with a diameter of 1.5 mm resulting in reinforcing ratio of 0.4 vol%. The billet temperature was set to 550°C. The profiles were extruded at a ram speed of 0.5 mm/s and an initial tool temperature of about 420°C, resulting, after natural ageing (>8 days at room temperature (RT)), in a T4 heat treatment state of the EN AW-6082 (AlMgSi1) matrix. Table 1 shows the chemical analysis of the used matrix alloy, measured by spectral analysis.

The composite wires used were manufactured via pressure infiltration at the TU Wien.[11] The composite wire consists of an AlMg0.6-matrix and Al_2O_3-fibers (Altex) with a typical chemical composition of 85 wt% Al_2O_3, 15 wt% SiO_2, and <0.005 wt% imperfections. The used composite wire was reinforced with ceramic fibers with a reinforcing ratio of 40 vol%. The ultimate tensile strength of the Al_2O_3-fibers was determined as 1860 ± 200 MPa by Doktor et al. As the tensile properties of the matrix were not accessible directly, the tensile strength was estimated from micro hardness measurements approximately as 128 MPa (30 HV0.01).

Experimental setup

Tensile tests. The tensile tests of the composite wires, the non-reinforced matrix material and the composite wire reinforced composite specimens were performed at RT on a ZWICK 200 kN electro mechanical universal testing machine at a crosshead velocity of 1 mm/min for the specimens and 1.5 mm/min for the composite wire. The gauge length was 100 mm for the composite wires and 25 mm for the pure and reinforced matrix material, which is conform to DIN EN 2002[17] for quasi-static tensile tests for bulk material and wires. The composite specimens were flat test specimen with a section of $3.1 \times 5\,mm^2$ resulting in a composite wire volume fraction of 11.4 vol% which is equal to a fiber fraction of 4.5 vol% in the specimen. The specimen manufacturing was done by a milling process. The strain was measured with an extensometer and additionally with an optical strain measurement system (GOM) for analyzing global and local strain distributions (Figure 3a).

In situ μ-CT tensile tests. The in situ tensile tests in the CT of the hybrid composite specimens were done with a self-designed setup which is capable of applying a maximum load of 5 kN according to Figure 3b. This setup is driven by a stepper motor which was also used to measure the crosshead displacement and a recirculating ballscrew placed central in the crosshead. In order to achieve a low x-ray absorption a CFRP tube was used as a support structure for the upper crosshead. Due to the small diameter of the tube (40 mm) the distance between the X-ray source and the sample could be kept small which allowed a high geometrical magnification. The low total weight of 14.5 kg allowed a direct mounting on the CT goniometer. Crosshead velocity was set to 1 mm/min. Prior to scanning a holding time of about 20 min was established to allow the system for setting in and avoid aberrations during scanning on specific damage events. As the imaging unit, an Yxlon-CT precision CT with an open micro-focus X-ray transmission tube (tungsten target) and a flat panel detector with 2048 x 2048 pixels from Perkin Elmer® were used. All tests were performed in the absorption method. The accelerating voltage was set to 125 kV and the accelerating current to 0.01 mA. The recording time of one scan was approximately 1 h. Avizo® Fire from VSG and ImageJ® were used for the image analysis.

Hardness measurements. Vickers micro hardness measurements were performed in the composite wire matrix and the profile matrix using a QNESS Q10 automatic micro hardness measurement system. For each sample five measurements were conducted. The test load was chosen to 10 g with a loading time of 10 s.

Results

Microstructure

Figure 4 depicts the microstructure of the composite wire, which was embedded in an epoxy matrix for metallographic preparation, before (left) and the hybrid

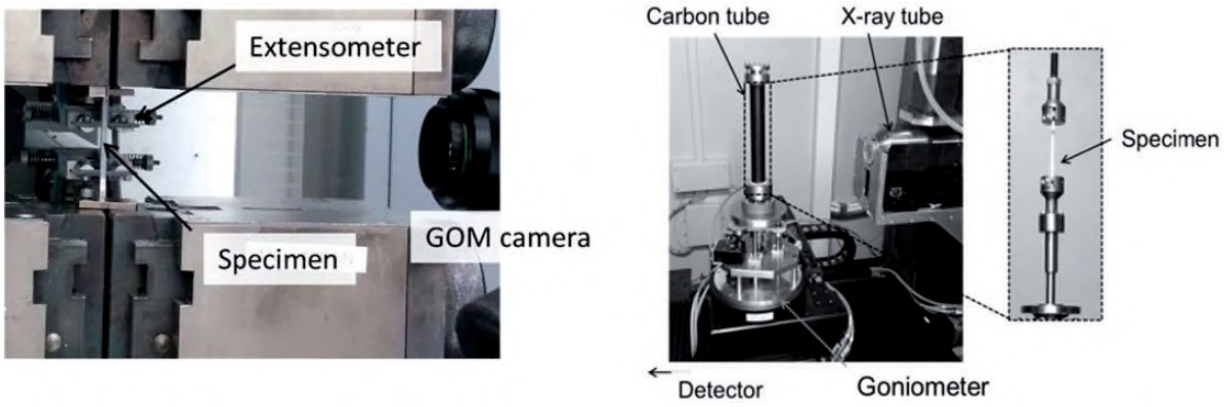

Figure 3. Experimental setup for a) tensile testing and b) in situ μ-CT tensile testing.

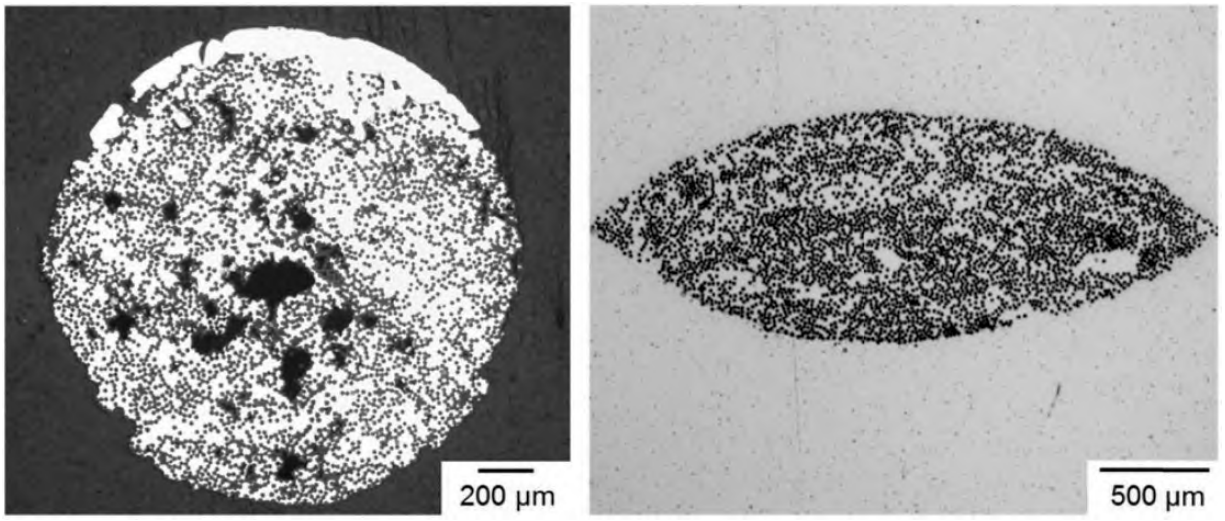

Figure 4. Microstructure of the composite wire (initial state) (left) and hybrid composite after extrusion (right).

composite after the composite extrusion process (right). It is visible that the initial round and porous state of the composite wire is transformed in an ellipsoid form with a significant reduction of porosity. The initial porosity can be related to the infiltration process, which could be due to low infiltration pressure[18,19] or lack of ultrasonic support.[20,21] The ellipsoid deformation can lead back to the flattening of the composite wire during joining of two matrix material strands within the welding chamber. The interface between profile matrix and composite wire shows a very good bonding, as expected. The border between the AlMg0.6-alloy and the EN AW-6082-alloy can be distinguished by examining the precipitations which only form in the hardenable EN AW-6082-alloy. The distribution of the Altex-fibers is inhomogeneous, with areas of fiber agglomeration and areas without fibers, as seen in the composite wire prior to extrusion.

Figure 5 shows the microstructure after a barker etching of the composite wire (left) and the hybrid composite (right) with deformed wire and AlMgSi1-matrix. The mean grain size was determined by an intercept procedure. The composite wire shows a relative coarse grain formation with grain sizes of about 104.6 μm. After composite extrusion the microstructure is characterized by very fine grains of the AlMgSi1-matrix, with grain sizes of about 21.7 μm, and coarse grains in the composite wire, where the grain size gets slightly finer with a mean grain size of 34.2 μm, which is assumed to be a result from dynamic recrystallization of the AlMg0.6 alloy due to hot deformation during composite extrusion.[22–24]

Mechanical properties

Figure 6 (left) depicts the stress–strain curve of the composite wire. It can be seen that the ductility of the wire is low with a total strain to fracture of about 1.2%.

Figure 6 right shows representative stress–strain diagrams for the hybrid composite and the unreinforced

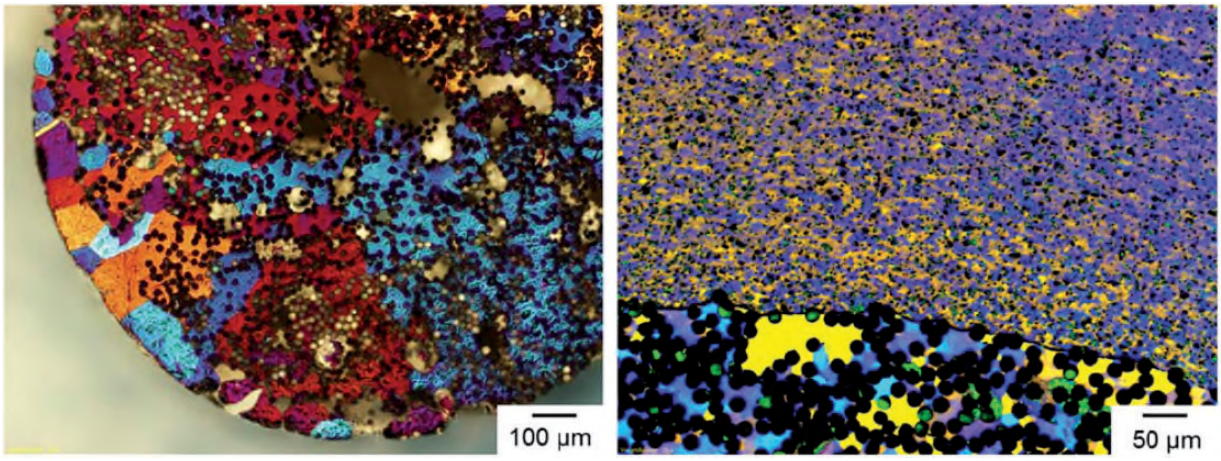

Figure 5. Microstructure of the composite wire (initial state) (left) and hybrid composite after extrusion (right).

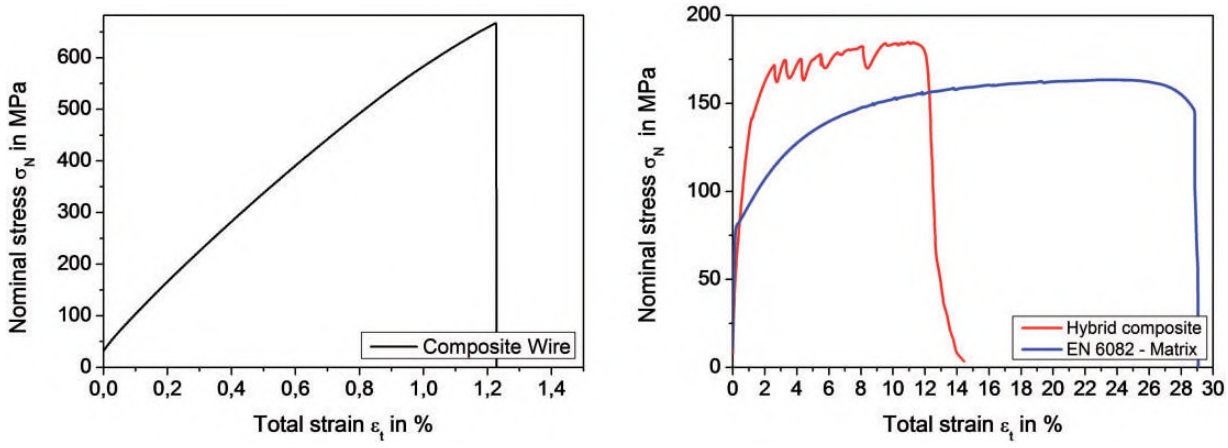

Figure 6. Exemplary stress–strain diagram (left) and comparison of mechanical properties (right).

matrix material. It can be seen that the ultimate tensile strength of the composite exceeds the strength of the unreinforced material and the strain to failure is reduced at the same time. It is obvious that the slope of the composite is slightly smaller than that of the unreinforced material, which could lead back to an initial bending of the tensile specimen due to large residual stresses in the composite. These residual stresses result from the large difference in thermal expansion between the composite wires and the aluminum matrix. For this reason no further conclusions could be drawn regarding the specimen stiffness. At a total strain of 2.6% a first stress drop occurs as a result composite wire failure, which implies a significantly higher strain to fracture as the single composite wire. Afterwards a region can be distinguished where strain hardening of the specimen with multiple load drops in between occurs, leading to the failure of the specimen at a total strain of about 12.3%. The curve progression of the composite after the first fracture of the composite wire is rather particular and needs further investigations which are introduced in "Deformation and damage analysis" section.

Table 2 gives an overview of the strength ($\sigma_{p0.2}$, σ_{UTS}) and the total strain to fracture. It can be concluded that the 0.2%-offset yield strength can be increased by 16%; the ultimate tensile strength is increased by 13.2%. The strain to fracture is reduced by 60.4%. As the density of the composite is increased only by less than 1%, the measured improvement in absolute strength values corresponds roughly to the increase in specific properties.

Deformation and damage analysis

The deformation and damage analysis included fractographic SEM investigations, as well as optical strain analysis and CT analysis.

Fractographic investigations. Figure 7 shows SEM images taken from the fracture surfaces of a composite

Table 2. Measured mechanical properties of components and hybrid composite material.

	$\sigma_{p0.2}$ (MPa)	σ_{UTS} (MPa)	$\varepsilon_{t,f}$ (%)	$\frac{\sigma_{p0.2}}{\rho}\left(\frac{MPa}{kg/m^3}\right)$	$\frac{\sigma_{p0.2}}{\rho}\left(\frac{MPa}{kg/m^3}\right)$
Altex-composite wire	–	725.0 ± 47.9	1.2 ± 0.1	–	250
EN AW-6082 matrix	83.4 ± 0.1	163 ± 0.5	28.6 ± 0.3	30.9	60.4
Hybrid composite Altex/6082	96.7 ± 0.2	184.5 ± 0.3	11.1 ± 1.7	35.5	67.6

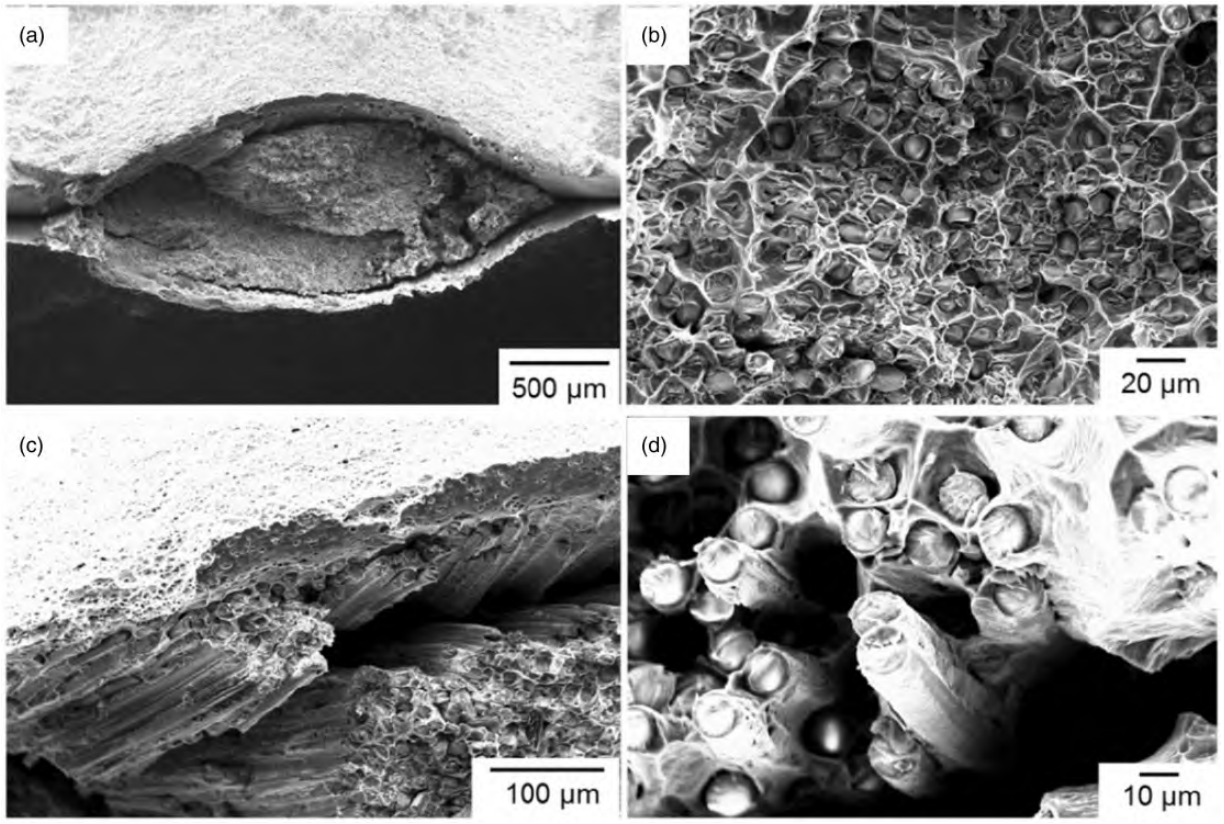

Figure 7. Fractographic analysis: a) fracture surface of the composite wire, b) magnification of fracture surface, c) interface between composite wire matrix and extrusion matrix, and d) magnification of fiber surface.

specimen. Figure 7a shows the composite wire with surrounding matrix. It can be seen that the fracture of the composite wire takes place in one plane and a deformation of the matrix around the fracture plane occurs. Furthermore it can be found that the longitudinal weld seam in combination with the elliptical shape of the wire leads to a delamination along the weld seam determining it as a critical point for composite failure as seen before in steel wire reinforced aluminum extrusions.[6] Figure 7b shows the magnification of the surface area. Here the high plasticity of the composite wire matrix can be derived from the ''honeycomb'' formation around the fibers, which indicates a fracture of them prior to fracture of the composite wire matrix and a good interface bonding. Almost no pull-out of fibers could be observed.

Figure 7c shows the debonded interface area between composite wire and extrusion profile matrix. It is visible that a large part of Al_2O_3-fibers (including the composite wire matrix between them) stick on the side of the EN AW-6082-Matrix. This reveals that the damage at the interface mostly takes place in the composite wire and the bonding between composite wire and EN AW-6082 matrix is very good. Figure 7d shows a close-up of some fiber surfaces. Most of the fibers are covered with aluminum which also indicates a good bonding between Al_2O_3-fibers and AlMg0.6-matrix.

Optical strain analysis. Figure 8a–d shows the results of the optical strain measurements during tensile testing (Figure 6 right) according to the x-position in the

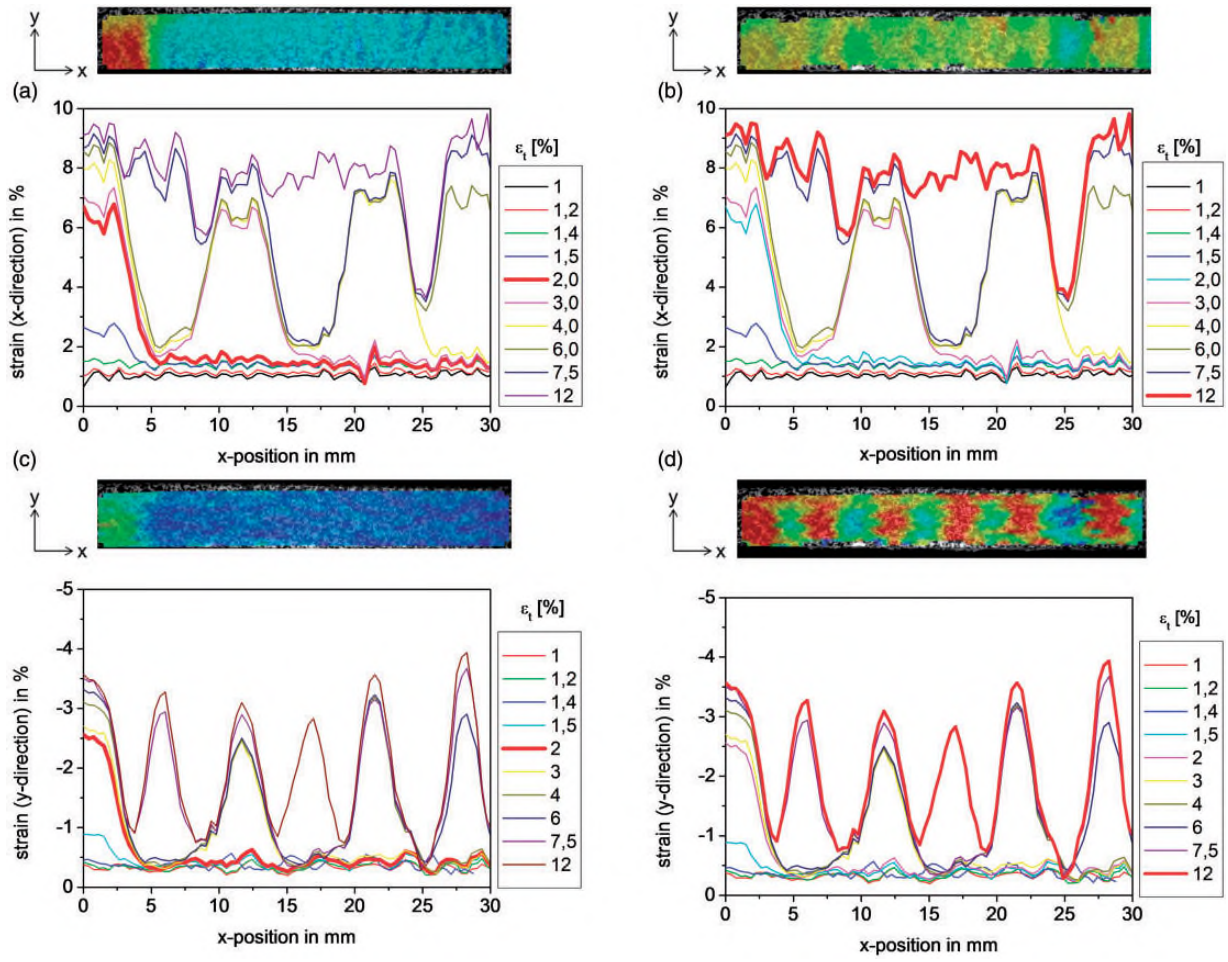

Figure 8. Strain distribution in longitudinal (x-direction) and transversal (y-direction) at first fracture ($\varepsilon_t = 2\%$) (left) and after before ultimate failure ($\varepsilon_t = 12\%$) (right).

measurement length. Figure 8a and b depicts the longitudinal strain evolution in the specimen (x-direction). The point of first wire fracture ($\varepsilon_t = 2.0\%$) and a point shortly before ultimate specimen failure ($\varepsilon_t = 12.0\%$) are highlighted in the diagrams. Figure 8c and d depicts the devolution of the corresponding transversal strains (y-direction). In addition the pictures above the diagrams offer a visualization of the local strain distribution in the measurement length.

It can be derived from the diagrams that corresponding to wire fracture a localized zone of deformation around the fracture point establishes. The longitudinal deformation then only takes place in this zone, thus resulting in localization also in transversal direction (necking). Subsequent further fractures of the wire lead to the formation of further localized zones of deformation, causing a multiple necking of the specimen (c). In the end prior to specimen failure ($\varepsilon_t = 12.0\%$) the elongation of the specimen in x-direction is almost homogenous. At one point ($x = 25\,\text{mm}$) the elongation is clearly smaller. The deformation in y-direction at $\varepsilon_t = 12.0\%$ shows six definite zones in the measurement length which can be correlated to the points of wire fracture derived from the devolution of the longitudinal strain (multiple necking). Also here the curve shows a singularity at $x = 25\,\text{mm}$ with almost no deformation. Final fracture of the specimen occurred at $x = 4\,\text{mm}$. The fact that a strain hardening after wire fracture can be seen in the stress–strain curve leads to the assumption that hardening takes places in the vicinity of the fracture point of the wire and therefore enables a load transfer (bridging effect) over the fracture point into the remaining part of the specimen. This mechanism continuously progresses as long as the fiber fragment length exceeds the critical fiber length of the system, which is determined by the ultimate tensile strength of the composite wire and its bonding with the surrounding matrix (interface shear strength).

In situ μ-CT tensile tests. In order to verify the assumed damage mechanisms and clarify the inner damage evolution of the composite wire, in situ CT analyzes were

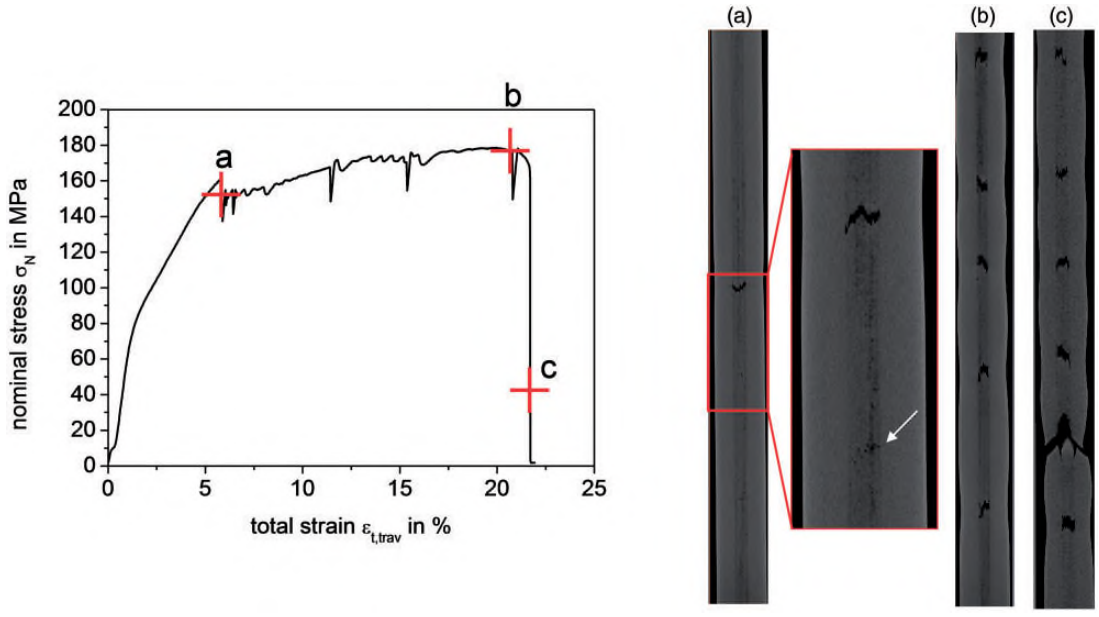

Figure 9. μ-CT In situ test: the tensile test was stopped for CT-imaging a) after first load drop, b) before ultimate specimen failure, and c) after failure.

made. Figure 9 (left) shows the determined stress–strain diagram from the in situ tensile testing. The apparent large load drops correlate with the stopping points for CT imaging and were lead back to setting effects. The load drops due to wire fracture were therefore relatively small, so not all fracture points could be detected. Figure 9a shows the specimen after first wire fracture and following hardening (according to Figure 6). It can be seen that the internal fracture of the composite wire takes place in one flat fracture plane (according to Figure 6a).

Furthermore the second point of wire fracture can be observed in its beginning. It can be concluded that the wire fracture is initialized by fracture of fibers (arrow). The accumulation of fiber fractures in one plane confirms a local load distribution during fiber fracture. The following damage accumulation can be summarized by the formation of further fractures of the composite wire with simultaneous multiple necking and further interface damage causing a debonding of the composite wire on all fracture points (Figure 8b and c) up to the final failure of the specimen.

Derivation of interfacial shear strength from damage behavior. As the investigated material shows a fragmentation of the reinforcement wire inside the composite, a derivation of the interfacial shear strength, similar to a single fiber fragmentation test,[25] which is often used for fiber reinforced plastics, can be done. If the critical fiber fragment length is reached no further force transmission beyond the tensile strength of the wire is possible and no further fragmentation of the wire is possible, therefore the average shear strength at the interface can be estimated from a simple force balance equation for a constant interfacial shear stress[26]:

$$\tau_{IS} = \frac{\sigma_f^{RE} \cdot d}{2l_c} \tag{1}$$

$$l_c = \tfrac{4}{3}\bar{l} \tag{2}$$

where σ_f^{RE} is the strength of the reinforcing element at the critical length, d is the fiber diameter, l_c is the critical fiber length, and $\bar{l}$ is the average fragment length.

Using these equations (the circumference of the wire remains constant), the critical fracture length was determined by optical analysis to 6.13 ± 1.6 mm which means an average shear strength of $\tau_{GF} = 93 \pm 25$ MPa. The CT analysis shows a critical fiber length of about 6.4 mm which equals a shear strength of 85 MPa and is in good agreement with optical strain measurements.

As the determination of the mechanical properties of the EN AW-6082/AlMg0.6 interface is difficult, a comparison with the shear strength of the weakest partner (AlMg0.6) is reasonable, hence the maximum interface shear strength cannot exceed the shear strength of the AlMg0.6 of the composite wire matrix. As the direct measurement of the ultimate tensile strength and the shear strength of the AlMg0.6 matrix is not possible, micro hardness measurements were made and

according to DIN EN ISO 18265[27] and Davis[28] converted into estimated shear strength:

$$\tau_{USS} \approx \alpha_{HB} \cdot \gamma_{USS} \cdot HV \quad (3)$$

with the conversion coefficients $\alpha_{HB} = 0.95$[27] and $\gamma_{USS} = 3.9$.[28] The measured hardness of the composite wire matrix was 30 HV0.01 ± 3.5 which leads to an estimated shear strength of 88.8 ± 10.3 MPa. As the used translations are basically of an empirical manner, this value can only serve as a rough comparative value, but nevertheless shows a good agreement to the interfacial shear strength which was deduced from the tensile tests.

Summary and conclusion

- Manufacturing of hybrid composite profiles:

  The investigations showed that the composite extrusion process with composite wires is a feasible way to manufacture composite profiles with ceramic reinforcement as shown on a system consisting of a hardenable aluminum matrix reinforced with Al_2O_3/Al-composite wires. Due to the high pressure during extrusion a deformation of the composite wire is observed, accompanied by a densification of the wire, which eliminates initial porosities occurring during the infiltration process of the ceramic wires.

- Mechanical properties:

  The mechanical performance showed an increase in specific strength and a reduction of strain to failure. The strain to failure was much higher than assumed by the strain to fracture of the composite wire in particular and could be explained by the deformation and damage behavior of the composite. Although the specific stiffness could not be measured due to specimen deformation during specimen manufacturing an increase in stiffness is expected, as the composite wire shows an excellent bonding, according to the derived interface shear strength (''In situ μ-CT tensile tests'' section) and a full load transfer during elastic deformation can be assumed. For determining the composite stiffness in further investigations the specimen geometry and manufacturing (e.g. cylindrical specimen and turning instead of milling) has to be adjusted to ensure an exact alignment of the composite wire in the specimen and avoid bending of the specimen due to the residual stresses in the composite.

- Deformation and damage behavior:

  The deformation and damage behavior showed a multiple fracture of the composite wire with subsequent multiple necking of the hybrid composite specimen in the measurement length. Further analysis of the multiple necking by optical strain measurement and in situ computer tomography allowed a detailed characterization of the occurring damage mechanisms, which were lead back to a stepwise multiple fracture of the composite wire with corresponding localization of deformation around the fracture zone. The subsequent damage mechanism is then characterized by interface debonding and multiple necking of the specimen leading to the final failure of the specimen as seen in the CT analysis. Furthermore it could be confirmed that the fracture of the composite wire is initialized by ceramic fiber fracture while local load transferring leads to a flat wire fracture.

- Correlation of interface shear strength:

  As the final fragment length can be correlated to a critical fiber length, an estimation of the wire–matrix interface shear strength was possible. These calculations confirmed the good bonding of the interface as assumed from the metallographic and fractographic investigations before. Compared to the shear strength of the composite wire matrix, which was calculated from hardness measurements in the composite wire matrix, the determined interfacial shear strength is in good agreement with the shear strength of the composite wire matrix (AlMg0.6). This confirms the applicability of this single fiber fragmentation method for determining the interface shear strength between composite wire and surrounding matrix in the investigated material system.

The introduced investigations in this contribution reveal the possibilities of ceramic reinforcement of aluminum profiles using a composite extrusion process. This process is a promising way for producing new high performance materials. Although the composite wire used was of relative low quality a significant increase of the specific strength properties could be attested. Even so the absolute mechanical properties are not outstanding yet, a further improvement is expected using composite wires with high strength and high moduli ceramic fibers (e.g. Nextel 610 fibers) and higher volume fraction of fibers.[14]

Acknowledgment

The authors wish to thank subproject A2 of the Transregional Collaborative Research Center/Transregio 10 for manufacturing of the composite profiles and Prof Degischer from the Institute of Material Science and Material Technology (TU WIEN) for providing the composite wire samples.

Conflict of interest

None declared.

Funding

This paper is based on investigations of the subproject A3—"Material systems for reinforced and functional extruded profiles"—of the Transregional Collaborative Research Center/Transregio 10, which is kindly supported by the German Research Foundation (DFG).

References

1. Schomäcker M, Schikorra M and Kleiner M. In: *4 years of research on composite extrusion for continuous reinforcement of profiles, conference: aluminium two thousand*, Florence, Italy, 13–17 March 2007.
2. Klaus A, Schomäcker M and Kleiner M. First advances in the manufacture of composite extrusions for lightweight constructions. *Light Metal Age* 2004; 62: 12–21.
3. Weidenmann KA, Fleck C, Schulze V, et al. Materials selection process for compound-extruded aluminium matrix composites. *Adv Eng Mater* 2005; 7: S1150–1155.
4. Weidenmann KA, Kerscher E, Schulze V, et al. Mechanical properties of compound-extruded aluminum-matrix profiles under quasi-static loading conditions. *Adv Mater Res* 2006; 10: 23–24.
5. Merzkirch M, Reeb A, Weidenmann KA, et al. Charakterisierung des Verformungs- und Schädigungsverhaltens unidirektional drahtverstärkter aluminium- und magnesiummatrixverbunde unter Zug und Druckbeanspruchung. In: Wielage, Bernhard (Hrsg.): Tagungsband zum 18. In: *Symposium Verbundwerkstoffe und Werkstoffverbunde*, Chemnitz, 30 March–1 April 2011.
6. Merzkirch M, Meissner M, Schulze V, et al. Tensile behaviour of spring steel wire reinforced EN AW-6082. *J Compos Mater* 2015; 49: 261–274.
7. Merzkirch M, Meissner M, Schulze V, et al. Numerical analysis to study the tensile behaviour of a spring-steel-wire-reinforced aluminium alloy metal matrix composite. *J Compos Mater* 2015; 49: 2659–2671.
8. Merzkirch M, Reeb A, Schulze V, et al. Cyclic deformation and damage behaviour of the spring steel wire reinforced aluminum alloy EN AW-6082. *J Mater Sci* 2014; 49: 2187–2203.
9. Reeb A, Schweizer L, Weidenmann KA, et al. Characterization of unreinforced and steel wire reinforced magnesium alloy AZ31 under mechanical-corrosive loading. *Proc CIRP* 2014; 18: 114–119.
10. Löhe D, Schulze V, Fleck C, et al. Verbundstranggepresste Aluminiummatrixverbunde – Werkstoffauswahl und Charakterisierung ausgewählter Metall-Metall-Systeme. *Aluminium, 80*. Jahrgang 2004; 12: 1374–1378.
11. Doktor M, Blucher J and Degischer HP. Continuous fiber reinforced aluminium wires. In: *ICCM-12*, Paris, 5–9 July 1999.
12. Blucher JT and Doktor M. A new pressure infiltration process for continuous production of fiber reinforced MMC structural elements. In: *Proceedings of the 30th international SAMPE technical conference*, San Antonio, TX, 22–24 October 1998, pp.442–449.
13. Weidenmann KA, Schomäcker M, Kerscher E, et al. Composite extrusion of aluminum matrix specimens reinforced with continuous ceramic fibres. *Light Metal Age* 2005; 63: 6–10.
14. Merzkirch M, Weidenmann KA, Kerscher E, et al. Mechanical properties of hybrid composite extrusions of an aluminum-alumina wire reinforced aluminium alloy. In: *Proceedings of materials science & technology conference and exhibition (MS&T'08)*, Pittsburgh, 5–9 October 2008, pp. 2552–2562.
15. Pietzka D, Schikorra M and Tekkaya AE. Embedding of alumina reinforcing elements in the composite extrusion process. *Adv Mater Res* 2008; 43: 9–16.
16. Dahnke C, Pietzka D, Haase M, et al. Extending the flexibility in the composite extrusion process. *Proc CIRP* 2014; 18: 33–38.
17. DIN EN 2002-001. *Metallic materials - Test methods – Part 1: Tensile testing at ambient temperature, Normenauschuss Luft- und Raumfahrt (NL)*, 2005.
18. Kientzl I, Németh Á and Dobránszky J. Influence of the infiltration pressure on the properties of MMC wires. *Mech Eng* 2008; 52/1: 15–18.
19. Kientzl I and Dobránszky J. Production and behaviour of aluminium matrix double composite structures. *Mater Sci Forum* 2008; 589: 105–110.
20. Matsunaga T, Ogata K, Hatayama T, et al. Effect of acoustic cavitation on ease of infiltration of molten aluminum alloys into carbon fiber bundles using ultrasonic infiltration method. *Compos Part A* 2007; 38: 771–778.
21. Matsunaga T, Ogata K, Hatayama T, et al. Fabrication of continuous carbon fiber-reinforced aluminum-magnesium alloy composite wires using ultrasonic infiltration method. *Compos Part A* 2007; 38: 1902–1911.
22. Humphreys FJ and Hatherly M. *Recrystallization and related annealing phenomena*. Oxford: Pergamon. 1996. ISBN: 0-08-041884-8.
23. Kannan K, Vetrano JS and Hamilton CH. Effects of alloy modification and thermomechanical processing on recrystallization of Al-Mg-Mn alloys. *Metall Mater Trans A* 1996; (22A).
24. Jazaeri H and Humphreys FJ. The transition from discontinuous recrystallization in some aluminium alloys II – annealing behaviour. *Acta Mater* 2004; 52: 3239–3250.
25. Feih S, Wonsyld K, Minzari D, et al. *Establishing a testing procedure for the single fiber fragmentation test*. Denmark: Forskningscenter Risø, 2004, 30 p. Risoe-R; No. 1483(EN).
26. Kelly A and Tyson WR. *Tensile properties of fibre-reinforced metals: copper/tungsten and copper/molybdenum*. 4th ed. London: Bowker-Saur, 1998, pp.51–55.
27. DIN EN ISO 18265, *Conversion of hardness values, Normenauschuss Materialprüfung (NMP)*, 2014.
28. Davis JR. *ASM specialty handbook: aluminum and aluminum alloys*. Materialspark, OH: ASM International Handbook Committee, 1993, ISBN: 978-0871704962.